JOURNAL OF COMPUTATIONAL PHYSICS **134,** 282–295 (1997)
ARTICLE NO. CP975695

Regularization of Two-Phase Flow Models: A Comparison of Numerical and Differential Approaches[1]

Himanshu Pokharna,* Michitsugu Mori,† and Victor H. Ransom*

*School of Nuclear Engineering, Purdue University, West Lafayette, Indiana 47907-1290; †Tokyo Electric Power Company, 1-1-3 Uchisaiwai-cho, Chiyada-ku, Tokyo 100, Japan
E-mail: ransom@ecn.purdue.edu

Received November 13, 1995; revised March 4, 1997

This paper illustrates the dominant role that numerical damping plays in the regularization of the two-phase flow models used in the RELAP5 and CATHARE codes. Dispersion analysis for a practical range of wave-number is used to examine the stability characteristics of both differential and numerical implementations of the two models. In this study it was found that numerical damping overshadows the effect of differential terms when they were added specifically to achieve a well-posed differential model such as is done for some flow regimes in the CATHARE code. Furthermore the added terms can result in non-physical dynamic behavior of the model. © 1997 Academic Press

1. INTRODUCTION

The process of regularization of otherwise ill-posed mathematical models for two-phase flow has continued to be a subject of concern since the first discovery that the inviscid two-fluid differential model for transient two-phase flow has complex characteristic roots and therefore is ill-posed as an initial value problem [1], except for the trivial case of equal phasic velocities. One reason that this problem has attracted so much interest is that it does not have a single-phase counterpart. By comparison, the analogous single-phase Euler model has real characteristic roots and is well-posed as an initial value problem.

The objective of this paper is to provide insight to the role that numerical regularization invariably plays in the process of modeling multiphase flows. This objective is achieved by using dispersion analysis to examine the approaches that are used for modeling two-phase flows in the RELAP5 and CATHARE light water reactor safety analysis codes. We will begin by examining the physical differences between single-phase and two-phase systems which complicate modeling, then briefly review the mathematical models used for two-phase flow and finally discuss the dynamic character of two models. To this latter end, we will present dispersion analysis results first for the RELAP5 and CATHARE differential models and then for the corresponding numerical models for each using a semi-implicit numerical scheme. The results of this analysis clearly reveal the dominant and necessary regularizing effect of the numerical scheme for both of these models.

1.1. *Physical Characteristics of Two-Phase Systems*

In comparison to single-phase systems, two-phase systems have added degrees of freedom which result in physical behavior not present in single-phase systems. The key difference is the presence of phasic interfaces having near discontinuous variation in the physical properties of the fluids and in the kinematics of the flow. These discontinuities result in manifestation of Rayleigh–Taylor and Kelvin–Helmholtz instabilities. Thus, it is reasonable to expect that a mathematical model for these processes might exhibit some temporal growth. However, we know from experience that physical damping and dissipation mechanisms limit the growth of instabilities when a system is isolated from external energy sources. Physical systems do not exhibit unlimited growth and thus neither should numerical models if they are to be useful models of physical systems.

The two principal mechanisms that provide stabilization in two-phase flows, particularly for short wavelength disturbances, are surface tension and viscosity. Surface tension provides a restoring force at interfaces and the viscosity results in dissipation of kinetic energy. Unfortunately the wavelength at which these processes become dominant or regularizing is much shorter than the wavelengths that can be resolved in numerical models for macroscopic systems, especially one-dimensional models. In such cases the numerical scheme must provide the required regularization, hopefully without significant effect on the long wavelength behavior.

[1] Work supported by Tokyo Electric Power Company, Japan.

0021-9991/97 $25.00
Copyright © 1997 by Academic Press
All rights of reproduction in any form reserved.

1.2. *Mathematical Modeling of Fluid Flow*

There are several avenues that have been explored for the mathematical modeling of fluid behavior. The most elementary is molecular dynamic modeling in which each molecule of the fluid is represented as a discrete entity and its instantaneous motion described by an appropriate set of dynamic equations. While this approach has been used for local modeling of two-phase interfaces, it is intractable for macro-scale problems, even in single-phase systems. In order to overcome the computational intractability of the molecular dynamic model for macro-scale systems, ensemble average formulations are employed to obtain continuum models such as the Navier-Stokes formulation for single-phase flow. The single phase continuum formulation has been extended to two-phase flow by modeling the interface as a discontinuity and developing the appropriate jump conditions that apply. This local instant model has been developed and recorded by Ishii [2] and others; however, the required explicit modeling of the interface again results in an intractable numerical problem for other than very simple situations and very few implementations of this model exist.

The local instant two-phase model can be again ensemble averaged over the phases or as an approximation, time and/or volume averaged [2, 3] to obtain a more tractable ''two-fluid'' model. The averaging process removes the interfacial details, but introduces the need for many new closure relationships. During the past two decades, this model has been the focus of an extensive effort to develop macro-scale numerical models for multi-phase flow. This basic two-fluid differential model has complex characteristic roots for algebraic closure models. Exact solutions for this model predict unphysical short wavelength behavior [1]. Certainly such a model poses a dilemma when numerical solution is considered since any numerical model must be stable in the von Neumann sense. Thus, either the differential model must be modified to more correctly describe the short wavelength physics of the process or a numerical scheme must be used that provides appropriate damping. The first approach poses a practical dilemma if the short wavelength process cannot be resolved by the numerical discretization. The objective of this research is to explore, by example, this interplay between modifying the differential model and/or the use of a stabilizing numerical scheme to obtain a well-posed numerical model. This objective is achieved by using dispersion analysis to establish the dynamic character of two contemporary differential models, i.e., the ones used in the RELAP5 and CATHARE codes. Subsequently we will again perform a dispersion analysis for a common numerical implementation of each model in order to separate the dynamic character of the numerical scheme from that of the differential models. In the two examples that are analyzed, a stabilizing differential closure relation is used only in the CATHARE model while numerical damping is common to both models. Thus we can deduce by comparison what effect the differential closure relationship has on regularization.

1.3. *Numerical Solution Methods*

All numerical processes have finite accuracy and noise in the form of truncation error is present at the scale of the discretization. Clearly if this numerical noise were permitted to grow it would soon dominate the solution and the results would be meaningless. Decay of the discretization noise is the basis for the von Neumann stability criterion which is a necessary condition for any successful numerical solution method. Regularization in the numerical sense requires that at least the shortest wavelength associated with the discretization must decay or be damped.

While it is necessary in any numerical process that the shortest wavelength decay, long wavelengths can grow if this is in agreement with the physics of the process. When long wavelength growth is present, a steady state can be achieved only if a nonlinear cascading process is present in which the long wavelength energy is ''cascaded'' to the short wavelengths so that decay occurs. Single-phase viscous flow is a classic case in which the differential model predicts that long wavelength instabilities are possible for sufficiently high Reynolds number even though the model is stable at short wavelengths where viscous dissipation is dominant. It has been empirically observed in turbulent single-phase flows that fluctuations or disturbances are initiated at the scale of the boundaries and that the unstable long wavelength disturbances not only grow but also cascade to short wavelengths by breaking up into smaller eddies. This cascade of energy to shorter wavelengths continues until the mean motion is stabilized by viscous dissipation of the turbulent kinetic energy. The lengthscale at which viscous effects become predominant is known as the Kolmogorov lengthscale [4]. However, turbulence modeling experience using large eddy simulation or subgrid scale modeling has shown that it is not necessary to use a spatial nodalization fine enough to resolve the Kolmogorov length-scale in order to achieve useful results [5]. With sufficient damping at wavelength and discretization interval much larger than the Kolmogorov scale, stability can be achieved without affecting the long wavelength behavior. There is an energy cascade from the long wavelength source to short wavelength sink. The acceptable cutoff must be empirically established, but for turbulent flow simulation it is found to be very much larger than the Kolmogorov lengthscale. Krishnamurthy and Ransom [6] present numerical evidence that this same phenomena occurs in the numerical modeling of two-phase flow which helps explain why existing methods that are in use, but based on an ill-posed differential model, work as well as they do.

1.4. *System Models*

When the behavior of an entire two-phase flow system such as a nuclear reactor primary side must be modeled, it is necessary to use one-dimensional models for most, if not all, of the flow paths. In a one-dimensional model the transverse gradients of axial velocity, which produce the dominant viscous shear and associated dissipation, cannot be represented and must be modeled. Likewise since the interface is not explicitly represented, it is not possible to include surface tension effects. The only dissipative mechanism in one-dimensional models is dilatational viscous stress (Arai [7]) which provides stability at very short wavelengths. However, the dilatational stress is not the dominant stress nor is it possible to use sufficiently fine discretization to resolve this stress. Thus, the dominant physical mechanisms for damping/dissipation of unstable modes cannot be represented and numerical or other artificial damping/dissipation mechanisms must be depended upon to stabilize an otherwise unstable model.

All successful numerical schemes for two-phase flow models by necessity include sufficient damping at the shortest wavelength of the discretization ($\lambda = 2\Delta x$) in order to achieve regularization whether physical dissipation and damping effects are explicitly modeled or not. The analysis and the conclusions that follow from this study are most directly applicable to the one-dimensional system model case. However, even if viscous shear is explicitly included in a multidimensional formulation, it is generally not feasible to use nodalizations fine enough to resolve the physical dissipation and stabilization mechanisms. Thus, the results of this study apply as well to the more general multidimensional case.

2. DISPERSION ANALYSIS OF THE DIFFERENTIAL MODELS

The approach taken in this research is to compare the dynamic character of two widely used differential models. Dispersion analyses are made for both the basic differential two-fluid model, used as a basis for the RELAP5 code and for a modified differential model used as the basis for the CATHARE code. The results for these two models are compared over a wide range of wave-number in order to clearly reveal differences of practical interest. The behavior of the CATHARE code model is also examined over an even wider range of wave-number in an effort to establish the wave number at which the added differential terms produce stability.

2.1. *The Basic Two-Fluid Differential Model*

We begin with the mean motion equations for two-phase flow [2, 3, 8] which are obtained from the local instant balance equations by temporal and/or spatial averaging. The one-dimensional system model is obtained as a special case. The resulting two-fluid model encompasses six field equations, the mass, momentum, and energy conservation equations for each phase. The averaged jump conditions are used to provide coupling between the phasic equations.

For the sake of simplicity and without loss of generality, an isothermal case without any phase change can be considered. Thus only a set of two equations for each phase remain. (It is well known that the energy equations do not affect the dynamic character of the two-phase flow equations, i.e., hyperbolic or not [9], and that the energy associated with the frictional dissipations is negligible). The specific mean flow equations which result for these approximations are given below.

Mass conservation,

$$\text{gas:} \quad \frac{\partial}{\partial t}(\alpha_g \rho_g) + \frac{\partial}{\partial x}(\alpha_g \rho_g v_g) = 0 \tag{1}$$

$$\text{liquid:} \quad \frac{\partial}{\partial t}(\alpha_f \rho_f) + \frac{\partial}{\partial x}(\alpha_f \rho_f v_f) = 0. \tag{2}$$

Momentum conservation,

$$\text{gas:} \quad \alpha_g \rho_g \frac{\partial v_g}{\partial t} + \alpha_g \rho_g v_g \frac{\partial v_g}{\partial x} = -\alpha_g \frac{\partial P}{\partial x} + \alpha_g \rho_g g - F_{wg} - F_I \tag{3}$$

$$\text{liquid:} \quad \alpha_f \rho_f \frac{\partial v_f}{\partial t} + \alpha_f \rho_f v_f \frac{\partial v_f}{\partial x} = -\alpha_f \frac{\partial P}{\partial x} + \alpha_f \rho_f g - F_{wf} + F_I. \tag{4}$$

Here α, ρ, and v are the averaged void fraction, density, and velocity, respectively. The subscripts g and f designate the gas and liquid phases, respectively. The pressure, P, is the average over both the phases. F_I is the volumetric interphase drag and F_{wg} and F_{wf} are the volumetric wall shear forces experienced by the gas and liquid phases, respectively. For this special case, the interphase momentum interaction F_I appears with opposite sign in the momentum conservation Eqs. (3) and (4).

The system of field equations is closed by inclusion of equations of state for the fluids. For the isothermal case, the equation of state for both the fluids is of the form, $\rho = \rho(P)$. Therefore we can write $\partial\rho/\partial t$ and $\partial\rho/\partial x$ in terms of the sound speed, c,

$$\frac{\partial \rho}{\partial t} = \frac{\partial \rho}{\partial P} \cdot \frac{\partial P}{\partial t} = \frac{1}{c^2} \frac{\partial P}{\partial t}$$

and

$$\frac{\partial \rho}{\partial x} = \frac{\partial \rho}{\partial P} \cdot \frac{\partial P}{\partial x} = \frac{1}{c^2} \frac{\partial P}{\partial x}. \tag{5}$$

The virtual mass term, normally included in the one-dimensional model, e.g., RELAP5 [10], has been omitted here for the sake of simplicity. The reason for this is that for the equation set considered (one pressure model), inclusion of the virtual mass force does not result in a hyperbolic model for all void fraction [11], and inclusion of these terms complicates the analysis without change to the conclusions.

Using $\alpha_f + \alpha_g = 1$, we can eliminate α_f from these equations and the remaining dependent variables for the system are α_g, P, v_g, and v_f. The system recast in terms of these variables is:

Continuity equations,

$$\rho_g \frac{\partial \alpha_g}{\partial t} + \frac{\alpha_g}{c_g^2}\frac{\partial P}{\partial t} + \rho_g v_g \frac{\partial \alpha_g}{\partial x} + \frac{\alpha_g}{c_g^2} v_g \frac{\partial P}{\partial x} + \alpha_g \rho_g \frac{\partial v_g}{\partial x} = 0 \quad (6)$$

$$-\rho_f \frac{\partial \alpha_g}{\partial t} + \frac{1-\alpha_g}{c_f^2}\frac{\partial P}{\partial t} - \rho_f v_f \frac{\partial \alpha_g}{\partial x} + \frac{1-\alpha_g}{c_f^2} v_f \frac{\partial P}{\partial x} + (1-\alpha_g)\rho_f \frac{\partial v_f}{\partial x} = 0. \quad (7)$$

The momentum equations remain the same as given by Eqs. (3) and (4). Constitutive relations assumed for the various drag forces are:

(a) *Interphase drag.* The following simple Darcy model is used for interphase drag. This expression is similar to that used in most of the existing codes and it is in agreement with the general structure proposed by Ishii and Zuber [12] for dispersed flows,

$$F_I = \frac{1}{2} C_d \rho_f (v_g - v_f) |v_g - v_f| \frac{A_p}{V}, \quad (8)$$

where A_p/V is the frontal area per unit volume. For a mono-dispersed bubbly flow, where the bubbles are assumed to be spheres of radius r_b, the frontal area per unit volume is $3\alpha_g/4r_b$. The drag coefficient, C_d, may be a function of α_g and the bubble radius. For this analysis, C_d is assumed constant. To eliminate the modulus operator, without loss of generality, both the phases are assumed to be moving in the positive x direction with $v_g > v_f$. Therefore, in terms of the basic variable set, we can write the interphase drag as

$$F_I = K_1 \alpha_g \rho_f (v_g - v_f)^2, \quad (9)$$

where K_1 is a constant.

(b) *Wall drag.* Again, a simple Darcy model with a multiplier is used. The resulting form of the relation is

$$\text{gas:} \quad F_{wg} = \frac{f_g}{2D} \rho_g v_g^2 A_{wg} = K_2 \rho_g v_g^2 \quad (10)$$

$$\text{liquid:} \quad F_{wf} = \frac{f_f}{2D} \rho_f v_f^2 A_{wf} = K_3 \rho_f v_f^2, \quad (11)$$

where f_g and f_f denote the gas and liquid friction factors, A's are the respective contact areas with the pipe wall, D is the pipe diameter, and the K's are constants.

We can now write the complete partial differential equation set of two continuity and two momentum conservation equations, in compact vector form as

$$\mathbf{A}\frac{\partial \boldsymbol{\phi}}{\partial t} + \mathbf{B}\frac{\partial \boldsymbol{\phi}}{\partial x} + \mathbf{C} = 0, \quad (12)$$

where $\boldsymbol{\phi} = [\alpha_g, P, v_g, v_f]^T$ is the vector of independent variables and $\mathbf{A}$, $\mathbf{B}$, and $\mathbf{C}$ are defined as

$$\mathbf{A} = \begin{bmatrix} \rho_g & \frac{\alpha_g}{c_g^2} & 0 & 0 \\ -\rho_f & \frac{1-\alpha_g}{c_f^2} & 0 & 0 \\ 0 & 0 & \alpha_g \rho_g & 0 \\ 0 & 0 & 0 & (1-\alpha_g)\rho_f \end{bmatrix} \quad (13)$$

$$\mathbf{B} = \begin{bmatrix} \rho_g v_g & \frac{\alpha_g}{c_g^2} v_g & \alpha_g \rho_g & 0 \\ -\rho_f v_f & \frac{1-\alpha_g}{c_f^2} v_f & 0 & (1-\alpha_g)\rho_f \\ 0 & \alpha_g & \alpha_g \rho_g v_g & 0 \\ 0 & (1-\alpha_g) & 0 & (1-\alpha_g)\rho_f v_f \end{bmatrix} \quad (14)$$

and

$$\mathbf{C} = \begin{bmatrix} 0 \\ 0 \\ -\alpha_g \rho_g g + K_2 \rho_g v_g^2 + K_1 \alpha_g \rho_f (v_g - v_f)^2 \\ -(1-\alpha_g)\rho_f g + K_3 \rho_f v_f^2 - K_1 \alpha_g \rho_f (v_g - v_f)^2 \end{bmatrix}. \quad (15)$$

2.2. *Dispersion Analysis for the Basic Two-Fluid Differential Model*

Dispersion analysis can be used to establish the dynamic character of a differential model over the frequency range of interest. Information regarding growth or decay of Fourier components and on the speed at which components of the solution are propagated can be obtained. Dispersion analysis provides greater insight into the dynamic character of a differential model than can be obtained from a characteristic analysis, which only provides information about the limiting short wavelength behavior ($\lambda = 0$). The effect of algebraic terms on the intermediate wavelengths can be studied by dispersion analysis whereas these terms do not affect characteristic analysis.

The dispersion relationship is obtained for a system of quasi-linear partial differential equations by linearizing the system about an initial state and using a general Fourier representation for each solution component. The local linear dynamic character of Eq. (12) can then be investigated by this method for a known state $\boldsymbol{\phi}^\circ$. The linear differential equation for the behavior of the perturbation, $\delta\boldsymbol{\phi} = \boldsymbol{\phi} - \boldsymbol{\phi}^\circ$ is

$$\mathbf{A}_\circ \frac{\partial \delta\boldsymbol{\phi}}{\partial t} + \mathbf{B}_\circ \frac{\partial \delta\boldsymbol{\phi}}{\partial x} + \left[\left(\frac{\partial \mathbf{A}}{\partial \boldsymbol{\phi}}\right)_\circ \cdot \left(\frac{\partial \boldsymbol{\phi}}{\partial t}\right)_\circ + \left(\frac{\partial \mathbf{B}}{\partial \boldsymbol{\phi}}\right)_\circ \cdot \left(\frac{\partial \boldsymbol{\phi}}{\partial x}\right)_\circ + \left(\frac{\partial \mathbf{C}}{\partial \boldsymbol{\phi}}\right)_\circ \right] \delta\boldsymbol{\phi} = 0. \tag{16}$$

Equation (16) defines the behavior of small perturbations $\delta\boldsymbol{\phi}$ about the unperturbed solution for instantaneous values of $\boldsymbol{\phi}^\circ$, $(\partial\boldsymbol{\phi}/\partial t)_\circ$, and $(\partial\boldsymbol{\phi}/\partial x)_\circ$. A solution in the form of a traveling wave is assumed,

$$\delta\boldsymbol{\phi} = \delta\boldsymbol{\phi}^\circ \exp[i(kx - \omega t)], \tag{17}$$

where k is the wave-number, ω is the complex frequency, and $\delta\boldsymbol{\phi}^\circ$ denotes the initial amplitude of the perturbation. On substitution of Eq. (17) into Eq. (16), a compatibility condition which $\delta\boldsymbol{\phi}^\circ$ must satisfy is obtained:

$$-i\omega\mathbf{A}\delta\boldsymbol{\phi}^\circ + ik\mathbf{B}\delta\boldsymbol{\phi}^\circ + \left[\left(\frac{\partial \mathbf{A}}{\partial \boldsymbol{\phi}}\right)_\circ \left(\frac{\partial \boldsymbol{\phi}}{\partial t}\right)_\circ + \left(\frac{\partial \mathbf{B}}{\partial \boldsymbol{\phi}}\right)_\circ \left(\frac{\partial \boldsymbol{\phi}}{\partial x}\right)_\circ + \left(\frac{\partial \mathbf{C}}{\partial \boldsymbol{\phi}}\right)_\circ \right] \delta\boldsymbol{\phi}^\circ = 0. \tag{18}$$

Equation (18) is a homogeneous linear system of equations which determines the components of $\delta\boldsymbol{\phi}^\circ$. The condition under which nontrivial solutions for $\delta\boldsymbol{\phi}^\circ$ exist is that the determinant of the coefficient matrix must vanish; i.e.,

$$\det(-i\omega\mathbf{A} + ik\mathbf{B} + \mathbf{D}) = 0 \tag{19}$$

where

$$\mathbf{D} = \left(\frac{\partial \mathbf{A}}{\partial \boldsymbol{\phi}} \cdot \frac{\partial \boldsymbol{\phi}}{\partial t}\right)_\circ^{\mathrm{T}} + \left(\frac{\partial \mathbf{B}}{\partial \boldsymbol{\phi}} \cdot \frac{\partial \boldsymbol{\phi}}{\partial x}\right)_\circ^{\mathrm{T}} + \left(\frac{\partial \mathbf{C}}{\partial \boldsymbol{\phi}}\right)_\circ^{\mathrm{T}}. \tag{20}$$

For nonzero ω Eq. (19) can be written in a more insightful form as

$$\det\left[\mathbf{A} - \frac{k}{\omega}\mathbf{B} + \frac{k}{\omega}\cdot\frac{i}{k}\mathbf{D}\right] = 0. \tag{21}$$

For each real value of k, the above equation can be used to establish the corresponding values for k/ω. The imaginary part of ω (i.e., ω_{I}) will govern growth or decay depending on its sign and the real part (i.e., ω_{R}) yields the speed of propagation (ω_{R}/k) for the Fourier component corresponding to each k. Note that for finite k/ω in the limit as $k \to \infty$, Eq. (21) reduces to the characteristic equation corresponding to Eq. (12) and the k/ω values correspond to the characteristic eigenvalues.

For the basic two-fluid model, the matrices $\mathbf{A}$, $\mathbf{B}$, and $\mathbf{C}$ were given earlier. For the case of a perturbation wavelength much smaller than the lengthscale of the initial state or for an initial uniform steady state, $(\partial\boldsymbol{\phi}/\partial t)_\circ$ and $(\partial\boldsymbol{\phi}/\partial x)_\circ$ will be negligible or zero so that $\mathbf{D}$ becomes

$$\mathbf{D} = \left(\frac{\partial \mathbf{C}}{\partial \boldsymbol{\phi}}\right)_\circ^{\mathrm{T}}. \tag{22}$$

The elements of $\mathbf{D}$ are given by

$$\begin{aligned}
D_{11} &= D_{12} = D_{13} = D_{14} = 0 \\
D_{21} &= D_{22} = D_{23} = D_{24} = 0 \\
D_{31} &= -\rho_{\mathrm{g}} g + K_1 \rho_{\mathrm{f}} (v_{\mathrm{g}} - v_{\mathrm{f}})^2 \\
D_{32} &= -\frac{1}{c_{\mathrm{g}}^2}(\alpha_{\mathrm{g}} g - K_2 v_{\mathrm{g}}^2) + \frac{K_1}{c_{\mathrm{f}}^2}\alpha_{\mathrm{g}}(v_{\mathrm{g}} - v_{\mathrm{f}})^2 \\
D_{33} &= 2K_2 v_{\mathrm{g}} \rho_{\mathrm{g}} + 2K_1 \alpha_{\mathrm{g}} \rho_{\mathrm{f}} (v_{\mathrm{g}} - v_{\mathrm{f}}) \\
D_{34} &= -2K_1 \alpha_{\mathrm{g}} \rho_{\mathrm{f}} (v_{\mathrm{g}} - v_{\mathrm{f}}) \\
D_{41} &= \rho_{\mathrm{f}} g - K_1 \rho_{\mathrm{f}} (v_{\mathrm{g}} - v_{\mathrm{f}})^2 \\
D_{42} &= -\frac{1}{c_{\mathrm{f}}^2}[(1 - \alpha_{\mathrm{g}}) g - K_3 v_{\mathrm{f}}^2 + K_1 \alpha_{\mathrm{g}} (v_{\mathrm{g}} - v_{\mathrm{f}})^2] \\
D_{43} &= -2K_1 \alpha_{\mathrm{g}} (v_{\mathrm{g}} - v_{\mathrm{f}}) \rho_{\mathrm{f}} \\
D_{44} &= 2K_3 \rho_{\mathrm{f}} v_{\mathrm{f}} + 2K_1 \rho_{\mathrm{f}} \alpha_{\mathrm{g}} (v_{\mathrm{g}} - v_{\mathrm{f}}).
\end{aligned} \tag{23}$$

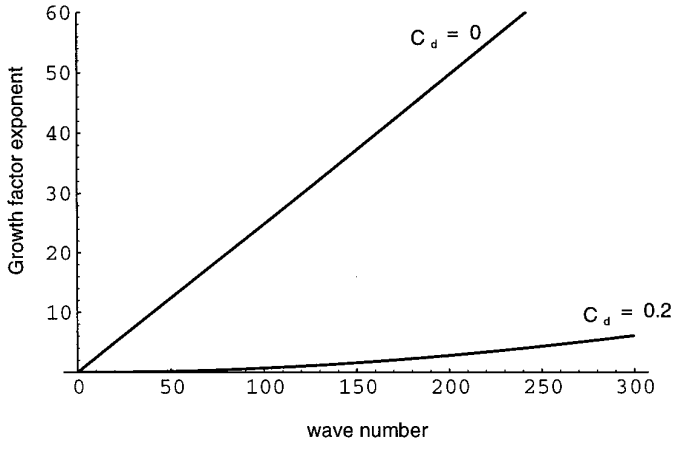

FIG. 1. Growth factor exponent for the basic two-fluid differential model for zero and 0.2 drag coefficients.

The roots of the quartic equation obtained by expanding Eq. (19) were determined using Mathematica. This analysis is complete in the sense that it accounts for interphase drag, wall drag, and compressibility effects. Exact solutions exist for the case of incompressible two-phase flow with zero interphase drag and zero wall friction and can be used as a check case. Ramshaw and Trapp [13] have shown that the growth factor for such a system is e^{ω_I}, where

$$\omega_I = \frac{|v_g - v_f|}{\alpha_g \rho_f + \alpha_f \rho_g} \sqrt{\alpha_g \alpha_f \rho_g \rho_f}\, k. \tag{24}$$

The model defined by Eq. (21) for the incompressible and zero drag case reduces to Eq. (24).

For all the calculations performed in this study, we have considered conditions typical of an idealized bubbly two-phase flow at a pressure of 10 MPa. The void fraction is assumed to be 0.1 and the liquid and vapor phases have velocities of 2.0 and 2.5 m/sec, respectively. For simplicity, the bubbles are idealized to be uniformly distributed and monosized with a diameter of 4 mm. Gravitational effects are assumed to be insignificant throughout this paper.

Figure 1 shows the variation of the maximum growth factor exponent, ω_I, with wave-number for both zero and finite drag ($C_d = 0$ and 0.2, respectively). A wave-number range from 0 to 300 ($0.02\ \text{m} < \lambda < \infty$) is used in order to cover a range well beyond that of practical numerical interest. This plot clearly shows that the ω_I remains positive even at high wave-number values. It is this positive, nonzero character of ω_I at all wavelengths of interest which has been a cause of spirited debates for over two decades about the acceptability of this model. In reality, viscous effects are a dissipative mechanism and provide a stabilizing effect. However, in the mathematical model the drag is modeled by an algebraic function which does not contain derivatives of the basic dependent variables. Thus the modeled drag does not enter into the expression for the calculation of the characteristic eigenvalues, i.e., at the limit as $k \to \infty$ and thus the modeled drag has no effect at high k. An important objective of the present study is to examine the solution behavior at component wavelengths of practical interest rather than just in the limit of zero wavelength (as is obtained from the characteristic analysis). A comparison of the growth factor exponents for zero and nonzero interphase drag reveals that inclusion of drag reduces the rate of growth. As we increase the interphase drag, the growth factor exponent decreases but never becomes zero. Thus, the basic unstable character (i.e., ω_I always remains positive) is not changed. This is shown more clearly by the surface plot in Fig. 2, where growth factor versus wave-number has been plotted for a range of interphase drag coefficient C_d from 0.0 to 1.0.

Physical systems do not exhibit unlimited growth at arbitrarily small wavelength and therefore the basic differential model does not correspond to real system behavior. This nonphysical behavior occurs because there are small wavelength physical phenomena which are not represented in the model. Neither the physical regularizing effects of surface tension nor viscosity are modeled. Furthermore, Ramshaw and Trapp [13] have shown, for the flow conditions that we have chosen in our example above, that the surface tension effect would only become a significant effect at wave-numbers above about 300 which is well beyond the range of practical node density. A spatial mesh size less than $\pi/300$ or $\sim$1 cm would be required to resolve components ($\lambda = 2\Delta x$) corresponding to this wave-number value. A node size this small, if used in a systems code for analyzing a nuclear reactor system, would result in a prohibitively

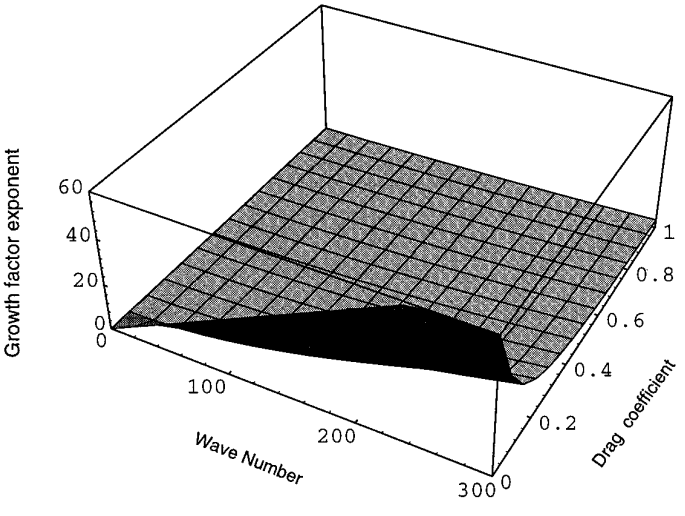

FIG. 2. Effect of drag coefficient on growth factor exponent for the basic two-fluid differential model.

large number of nodes. In addition, this lengthscale is generally much smaller than the characteristic dimension of the averaged two-fluid model, especially in one-dimensional formulations. Nevertheless, in order to investigate the differential regularization used in CATHARE over a wider range of wave-number, 300 is used as the upper limit of the wave-number for this study. This wave-number corresponds to a wavelength for the smallest component of 2 cm, i.e., $\lambda = 2\Delta x$.

Viscosity comes into play as a significant damping and dissipation mechanism at even higher wave-number than for surface tension. Thus, only if we artificially increase the value of surface tension (or viscosity), will models for these effects produce regularizing effects within a practical range of discretization interval.

2.3. *The CATHARE Code Differential Model*

In the formulation of the CATHARE code differential model, the developers have assumed, for the purpose of making the system of equations have real characteristic roots, that the interface between the two phases exists at a pressure different from an average phasic pressure. This is achieved by adding an interface pressure term to the gas momentum equation and subtracting it from the liquid momentum equation so that the mixture momentum equation is unchanged. The form of this term is given by Micaelli [14] and Bestion [15] as

$$I = (P - P_i)\frac{\partial \alpha_g}{\partial x}. \tag{25}$$

Where the minimum value for $P - P_i$ is modeled by

$$P - P_i = \frac{\alpha_g \rho_f (1 - \alpha_g)\rho_g}{\alpha_g \rho_f + (1 - \alpha_g)\rho_g}(v_g - v_f)^2. \tag{26}$$

Toumi [16] provided a development for this model with the objective being to obtain a hyperbolic system of equations, but no physical basis was proposed. The final form used for the pressure difference term is

$$P - P_i = \alpha_g \rho_f \delta (v_g - v_f)^2, \tag{27}$$

where the magnitude of δ, the so-called ''pressure coefficient,'' is chosen so as to make the system hyperbolic. δ is subsequently redefined as $\delta_o \varepsilon$, where δ_o is the minimum value of δ required to just make the system hyperbolic, and ε is a multiplier that should be greater than but close to one.

It should be noted that the CATHARE model has been derived assuming different values for liquid and gas phase pressures. However, in the end an average value of the pressures is substituted for the two pressures. Stuhmiller [17] has developed an expression for the interfacial pressure by integrating Lamb's expression for pressure distribution along the surface of a sphere. He obtained the added mass and the form drag terms as well as an expression for P_i similar to Eq. (27). Stuhmiller carried out his analysis assuming that the bulk pressures differed by a constant value due to surface tension so that his equation set which involved derivatives of the continuous phase pressures could be formulated in terms of a single pressure. If the virtual mass force is neglected from Stuhmiller's model, his equation set corresponds to that used for CATHARE; thus the present analysis will apply equally well to his model.

In reality the interfacial pressure difference defined by Eq. (27) is not applied in the CATHARE code for unstable stratified flow. In this case the interfacial pressure is derived from hydrostatic considerations. A similar formulation is used in the RELAP5 code for stratified flows. In this paper our aim is to study the effect of different regularizing terms in a global way and flow regime specific closure models such as for virtual mass effect and stratified flow have not been included. Thus only the interfacial pressure difference defined by Eq. (27) is used for study of the CATHARE differential model.

2.4. *Dispersion Analysis for the CATHARE Code Differential Model*

When a dispersion analysis is performed for the CATHARE equations, some of the coefficients of Eq. (12) must be modified to include the added differential terms that result from the model for $P - P_i$ given by Eq. (27). The altered values of the affected coefficients are

$$\begin{aligned} B_{31} &= \alpha_g \rho_f (v_g - v_f)^2 \delta \\ B_{41} &= -\alpha_g \rho_f (v_g - v_f)^2 \delta. \end{aligned} \tag{28}$$

The dispersion analysis method used to analyze the basic model (RELAP5) was repeated for this model. First the case of zero wall friction and zero interphase drag is considered. Flow conditions are the same as those described previously in Section 2.2. The numerical value of $\delta_o \varepsilon$ is assumed to be 0.45, whereas δ_o corresponding to these conditions is 0.44. Figure 3 shows the dispersion analysis results for this case. The growth factor exponent is zero at all wave-numbers for the case of zero interphase drag, $C_d = 0$. This is what is anticipated as the extra term $(P - P_i)(\partial \alpha_g / \partial x)$ is introduced so as to obtain real characteristics. However, for finite interphase drag, $C_d = 0.2$, the growth factor exponent is greater than zero for the range of wave-number studied.

Figure 4 shows a surface plot for the growth factor exponent versus wave-number for varying interphase drag coefficient. Here, the growth factor behavior for the CATHARE model is similar to that of the basic two-fluid model except for the zero drag case. Therefore, even for the CATHARE differential model, growth is always present in the wave-number range investigated even though the system becomes hyperbolic in the limit of infinite wave-number. By numerical exploration it was found that at ε slightly greater than 1 (i.e., $\delta_o\varepsilon = 0.45$ and $\delta_o = 0.44$), the wave-number at which the ω_I became zero (stable system) was of the order of 10^{20} which corresponds to shorter wavelength than that associated with any known physical effect. It was also observed that for higher values of ε, the growth factor exponent was correspondingly reduced. However, as ε is made larger, the model exhibits increasingly unphysical behavior. In a paper by Toumi [16], a solution for the CATHARE equations obtained using an approximate Riemann solver for a two-phase flow shock tube problem is reported. His calculations showed that at $\varepsilon = 10$, the solution for liquid and vapor phase velocities as well as energy develops some very unphysical spikes. These spikes were comparatively insignificant for $\varepsilon = 1.01$.

This result illustrates a danger of using a mathematical regularization that is not correct at all wavelengths, yet permits solutions to be obtained for arbitrarily high accuracy. The danger is that in an effort to prove convergence, solutions could be sought for short wavelength phenomena that are beyond the range of validity of the model. Such results can be unphysical yet be interpreted as accurate solutions for the basic differential model.

2.5. *Comparison of the Two Models*

First let us consider the idealized case of zero interphase and wall drag. As discussed previously, for this case and with nonzero relative velocity, ω_I linearly increases with k for the basic model. This is physically correct because in the absence of any stabilizing mechanisms (like gravity, surface-tension, or drag), the rate of growth corresponds to exact solutions for the Kelvin–Helmholtz instability [18]. The CATHARE differential model for the same idealized case, on the other hand, yields zero ω_I for all wave-numbers and thus the Kelvin–Helmholtz type instability is not predicted. This is clearly an unphysical stabilization for this idealized case.[2]

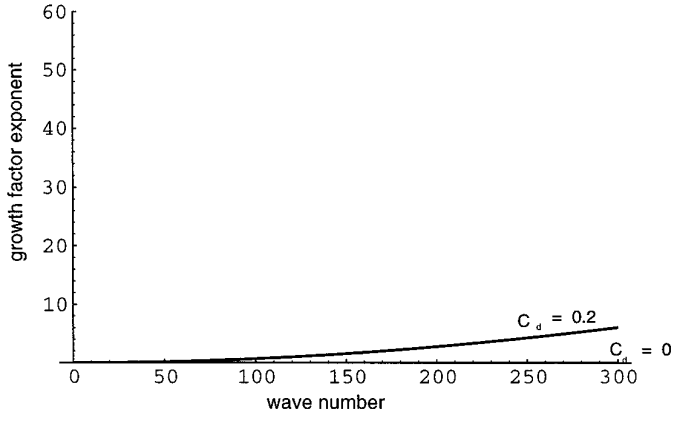

FIG. 3. Growth factor exponent for the CATHARE two-fluid differential model for zero and 0.2 drag coefficients.

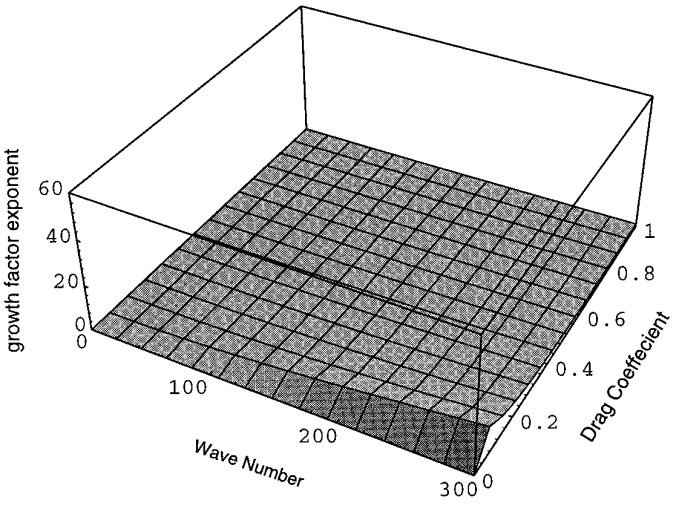

FIG. 4. Effect of drag coefficient on growth factor exponent for CATHARE two-fluid differential model.

At nonzero drag values, both the CATHARE model and the basic differential model show growth at all wavelengths of practical significance. However the CATHARE model does show lesser growth at all wavelengths. This can be observed by comparing the corresponding plots in Fig. 1 and Fig. 3.

An interesting result of this study is the effect of increasing the interphase drag coefficient on the growth factor exponent for the two different models. For the basic differential model as the drag coefficient value is increased at constant wave-number the growth factor becomes smaller, but for the CATHARE differential model the growth rate initially increases for small drag values, reaches a maximum, and then decreases with increase in drag as shown in Fig. 5 for a constant wave-number of 300. The growth factor exponent for the CATHARE differential model for the bubbly flow conditions assumed herein is again always lower than the basic model and the effect of interphase drag on the growth factor is nonmonotone.[3] However, if

[2] In the actual CATHARE code the interfacial pressure term is modified at those stratified flow conditions where flow can develop Kelvin–Helmholtz instabilities. This allows for growth in stratified flows.

[3] It was pointed out to us that similar results with regard to the CATHARE model were reported by de Crecy [19]. However, we were not able to obtain this reference.

the interfacial pressure term is not the same for dispersed liquid as for bubbly flows, this non-monotone character may be altered.

3. STABILITY ANALYSIS OF THE RELAP5 AND CATHARE NUMERICAL MODELS

Our main objective here is to demonstrate the dominant role that numerical damping plays in stabilizing two-phase numerical models in contrast to the effect of the differential terms introduced in the CATHARE model for this purpose. A von Neumann stability analysis similar to the dispersion analysis used to characterize the differential models is used to obtain growth rate versus wave-number for the RELAP5 and CATHARE differential models when both are combined with a semi-implicit numerical method. First the discretized system of equations are linearized with respect to the solution vector $\boldsymbol{\phi}$. Subsequently a recursion relation of the form $\boldsymbol{\phi}^{n+1} = [\mathbf{C}]\boldsymbol{\phi}^{n}$ is obtained. Linear stability theory requires that all the eigenvalues of $\mathbf{C}$ must be less than or equal to $1 + O(\delta t)$. For nonlinear systems intermediate growth factors may exceed this value; however, in all cases the growth factor at wavelength corresponding to $2\Delta x$ must satisfy this stability condition. As a practical criterion the stronger condition that the maximum eigenvalue be less than unity is usually applied.

3.1. *RELAP5 Numerical Model*

A difference approximation for the basic two-fluid model, Eq. (12), is used which is based on the semi-implicit numerical scheme with donor cell differencing for the convected terms. To keep a near one-to-one correspondence with the RELAP5 solution algorithm, the basic equation set is cast in sum and difference form [10] and the momentum flux terms are evaluated using a donor or upwind differencing scheme.

A staggered spatial nodalization is used in which computational control volumes for the scalar variables, P and α_g are denoted by an integer index, j. The velocity variables, v_g and v_f are located at the edges of the scalar control volume and are denoted by a fractional index, $j + \frac{1}{2}$. The difference equation corresponding to the differential balance equations are:

the mixture mass equation,

$$(\alpha_g\rho_g + \alpha_f\rho_f)_j^{n+1} - (\alpha_g\rho_g + \alpha_f\rho_f)_j^{n} + \{[\dot{\alpha}_g^n\dot{\rho}_g^n(v_g)_{j+1/2}^{n+1} + \dot{\alpha}_f^n\dot{\rho}_f^n(v_f)_{j+1/2}^{n+1}] - [\dot{\alpha}_g^n\dot{\rho}_g^n(v_g)_{j-1/2}^{n+1} + \dot{\alpha}_f^n\dot{\rho}_f^n(v_f)_{j-1/2}^{n+1}]\}\frac{\Delta t}{\Delta x} = 0, \tag{29}$$

the difference of phasic mass equation,

$$(\alpha_g\rho_g - \alpha_f\rho_f)_j^{n+1} - (\alpha_g\rho_g - \alpha_f\rho_f)_j^{n} + \{[\dot{\alpha}_g^n\dot{\rho}_g^n(v_g)_{j+1/2}^{n+1} - \dot{\alpha}_f^n\dot{\rho}_f^n(v_f)_{j+1/2}^{n+1}] - [\dot{\alpha}_g^n\dot{\rho}_g^n(v_g)_{j-1/2}^{n+1} - \dot{\alpha}_g^n\dot{\rho}_g^n(v_f)_{j-1/2}^{n+1}]\}\frac{\Delta t}{\Delta x} = 0, \tag{30}$$

the mixture momentum equation,

$$\begin{aligned}(\alpha_g\rho_g)_{j+1/2}^{n}(v_g^{n+1} - v_g^{n})_{j+1/2} + (\alpha_f\rho_f)_{j+1/2}^{n}(v_f^{n+1} - v_f^{n})_{j+1/2} \\ + \alpha_g\rho_g)_{j+1/2}^{n}v_{g_{j+1/2}}^{n}(v_{g_{j+1/2}} - v_{g_{j-1/2}})^{n}\frac{\Delta t}{\Delta x} \\ + (\alpha_f\rho_f)_{j+1/2}^{n}v_{f_{j+1/2}}^{n}(v_{f_{j+1/2}} - v_{f_{j-1/2}})^{n}\frac{\Delta t}{\Delta x} \\ = -(\mathrm{P}_{j+1}^{n+1} - \mathrm{P}_j^{n+1})\frac{\Delta t}{\Delta x} - \Delta t(\alpha_g\rho_g)_{j+1/2}^{n}\mathrm{FWG}_{j+1/2}^{n}v_{g_{j+1/2}}^{n+1} \\ - \Delta t(\alpha_f\rho_f)_{j+1/2}^{n}\mathrm{FWF}_{j+1/2}^{n}v_{f_{j+1/2}}^{n+1},\end{aligned} \tag{31}$$

the difference of phasic momentum equations,

$$\begin{aligned}[(v_g^{n+1} - v_g^{n}) - (v_f^{n+1} - v_f^{n})]_{j+1/2} \\ + (\alpha_g\rho_g)_{j+1/2}^{n}v_{g_{j+1/2}}^{n}(v_{g_{j+1/2}} - v_{g_{j-1/2}})^{n}\frac{\Delta t}{\Delta x} \\ - (\alpha_f\rho_f)_{j+1/2}^{n}v_{f_{j+1/2}}^{n}(v_{f_{j+1/2}} - v_{f_{j-1/2}})^{n}\frac{\Delta t}{\Delta x} \\ = \left[\frac{\rho_g - \rho_f}{\rho_g\rho_f}\right]_{j+1/2}^{n}(\mathrm{P}_{j+1/2}^{n+1} - \mathrm{P}_j^{n+1})\,\Delta t - \{\mathrm{FWG}_{j+1/2}^{n}v_{g_{j+1/2}}^{n+1} \\ - \mathrm{FWG}_{j+1/2}^{n}v_{f_{j+1/2}}^{n+1} + (\rho\mathrm{FI})_{j+1/2}^{n}(v_g - v_f^{n+1})_{j+1/2}\}\,\Delta t.\end{aligned} \tag{32}$$

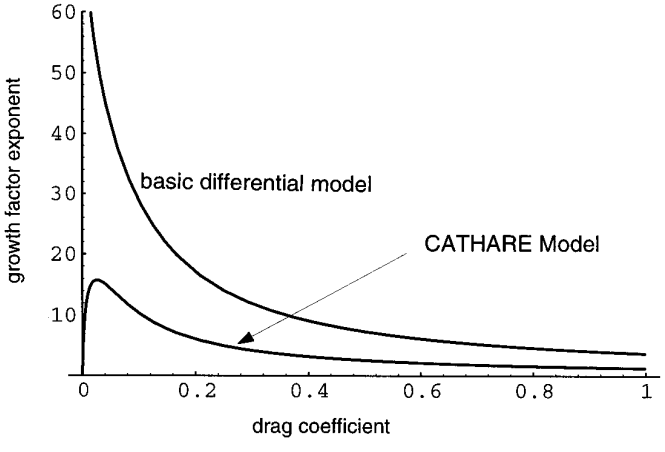

FIG. 5. Growth factor exponent versus drag coefficient for the basic and CATHARE two-fluid model at wave number 300.

The terms FWG, FWF, and FI designate the vapor and liquid wall friction and interphase friction coefficient, respectively. The superposed dot denotes a donored scalar quantity based on the vapor or liquid velocity.

In the actual RELAP5 numerical scheme, the convective term, $\alpha\rho v\ \partial v/\partial x$, is approximated by a combination of a central difference for the square of velocity and an artificial viscosity damping term. However, it can be shown that the RELAP5 approximation is equivalent to the upwind approximation for the momentum flux terms which is used here.

In order to apply the von Neumann stability analysis, the above difference equations must be expressed in terms of the four basic variables, α_g, P, v_g, and v_f. This is achieved by linearization of product terms in order to express the system of equations in terms of the primitive variables and then treating the coefficients of differences as constants over a time interval at a fixed spatial location.

The linearization procedure is illustrated for the product term appearing in the mass sum equation, i.e., for

$$\begin{aligned}(\alpha_g\rho_g)^{n+1} - (\alpha_g\rho_g)^n &= \alpha_g(\rho_g^{n+1} - \rho_g^n) + \rho_g(\alpha_g^{n+1} - \alpha_g^n)\\ &= \alpha_g \cdot \frac{1}{c_g^2}[P_g^{n+1} - P_g^n] + \rho_g(\alpha_g^{n+1} - \alpha_g^n)\end{aligned} \tag{33}$$

and similarly for

$$\begin{aligned}&(\alpha_{g_j}^n\rho_{g_j}^n v_{g_{j+1/2}}^{n+1}) - (\alpha_{g_{j-1}}^n\rho_{g_{j-1}}^n v_{g_{j-1/2}}^{n+1})\\ &\quad= (\alpha_g\rho_g)(v_{g_{j+1/2}} - v_{g_{j-1/2}})^{n+1} + \alpha_g v_g[\rho_j^n - \rho_{j-1}^n]\\ &\qquad+ \rho_g v_g(\alpha_{g_j}^n - \alpha_{g_{j-1}}^n)\\ &\quad= (\alpha_g\rho_g)[v_{g_{j+1/2}}^{n+1} - v_{g_{j-1/2}}^{n+1}] + \frac{\alpha_g v_g}{c_g^2}[P_j^n - P_{j-1}^n]\\ &\qquad+ \rho_g v_g(\alpha_{g_j}^n - \alpha_{g_{j-1}}^n).\end{aligned} \tag{34}$$

Substituting these relations into Eq. (29) and subsequently reordering the terms the following equation is obtained:

$$\begin{aligned}&\alpha_{g_j}^{n+1}[\rho_g - \rho_f] + P_j^{n+1}\left[\frac{\alpha_f}{c_f^2} + \frac{\alpha_g}{c_g^2}\right]\\ &\qquad+ v_{g_{j+1/2}}^{n+1}\left[\frac{\Delta t}{\Delta x}\alpha_g\rho_g(e^{ik\Delta x/2} - e^{-ik\Delta x/2})\right]\\ &\qquad+ v_{f_{j+1/2}}^{n+1}\left[\frac{\Delta t}{\Delta x}\alpha_f\rho_f(e^{ik\Delta x/2} - e^{-ik\Delta x/2})\right]\\ &\quad= \alpha_{g_j}^n\left[\rho_g - \rho_f - \rho_g v_g(1 - e^{-ik\Delta x})\frac{\Delta t}{\Delta x}\right.\\ &\qquad\left.+ \rho_f v_f(1 - e^{-ik\Delta x})\frac{\Delta t}{\Delta x}\right]\\ &\qquad+ P_j^n\left[\frac{\alpha_g}{c_g^2} + \frac{\alpha_f}{c_f^2} - \frac{v_g}{c_g^2}(1 - e^{-ik\Delta x})\frac{\Delta t}{\Delta x}\right.\\ &\qquad\left.- \frac{v_f}{c_f^2}(1 - e^{-ik\Delta x})\frac{\Delta t}{\Delta x}\right].\end{aligned} \tag{35}$$

Similarly, the remaining equations are linearized to obtain the following recursion expression relating values at time $t + \Delta t$ to values at time t,

$$\boldsymbol{\phi}^{n+1} = [\mathbf{A}]^{-1}[\mathbf{B}]\,\boldsymbol{\phi}^n \tag{36}$$

or

$$\boldsymbol{\phi}^{n+1} = [\mathbf{C}]\,\boldsymbol{\phi}^n, \tag{37}$$

where $[\mathbf{C}] = [\mathbf{A}]^{-1} \cdot [\mathbf{B}]$ is the amplification matrix. The vector $\boldsymbol{\phi}$, as defined previously is $[\alpha_g, P, v_g, v_f]^T$ and the elements of the matrices $\mathbf{A}$ and $\mathbf{B}$ are defined in the Appendix.

Due to inclusion of the interphase and wall drag terms, it is not possible to obtain an analytical result for the growth factor. Instead, Mathematica is used to numerically find the largest growth or decay factor, i.e., the largest eigenvalue of the amplification matrix over the range of numerical wavenumbers of interest. Extensive testing was performed for limiting cases of the problem in order to gain confidence in the solution procedure. For example, for void fractions of zero or one, the set of equations correspond to the single phase case where the semi-implicit scheme is known to be stable. Similarly, the case of equal velocities is known to be stable. These cases were verified.

3.2. *CATHARE Numerical Model*

In the actual CATHARE code, a fully implicit numerical scheme is used to solve the discretized equations. However, as our aim here is to study differences due to the added differential term used in the CATHARE model the same semi-implicit numerical solution procedure that was used for the RELAP5 analysis will be used for the CATHARE model. This provides a common basis for studying the effect of the interfacial pressure term added to the CATHARE model.

Differential terms which are common to both the models are finite differenced by the same method. For the additional term of the CATHARE model, $(P - P_i)(\partial\alpha_g/\partial x)$, an explicit difference scheme is used since this term does not affect the time step stability limit. Thus, with one exception the elements of the **A** and **B** matrices are the same as those for the RELAP5 case. The one new non zero term is:

$$B_{41} = -\alpha_g \rho_f \delta (v_g - v_f)^2 2(i) \sin \frac{k\Delta x}{2} \cdot \frac{\Delta t}{\Delta x} \left[\frac{1}{\rho_g \alpha_g} + \frac{1}{\rho_f \alpha_f} \right]. \tag{38}$$

Again, the limiting cases of zero and one void fraction, and zero relative velocity were verified to yield the known single phase results.

3.3. *Numerical Model Stability Comparisons*

In what follows, both the RELAP5 and the CATHARE numerical models are compared with the respective differential models using the growth factor modulus, e^{ω_I}, rather than just the exponent ω_I. For the stability analysis, the flow conditions assumed were the same as those previously used for the differential system dispersion analysis. In all cases, the time increment is such that the material Courant number based on the highest velocity (the gas phase velocity) is unity. This provides the most severe test of stability since increased numerical damping results for Courant numbers less than unity. For the purposes of establishing a range of wave-number for this study, a lower limit on computational node size of 0.1 m is assumed. This is about the lower limit of node size used in light water reactor transient simulation. This limit corresponds to a wave-number range from 0 to 10π in contrast to the larger range of wave-number from 0 to 300, which was used in the differential system study in order to investigate the high frequency character of the CATHARE differential regularization at wave-numbers well beyond the practical range.

For the idealized case of zero interphase and the wall drag, the CATHARE differential model exhibited the unphysical characteristic of zero growth at all wave-numbers. Thus it is not unexpected that the CATHARE numerical model also exhibits this same characteristic as shown in Fig. 6. However, the numerical model includes significant damping for wave-numbers greater than zero. In contrast, as shown before, the basic differential model of RELAP5 has growth factors that increase exponentially with wave-number while the numerical model shows growth for small wave-numbers, but becomes stable with increasing wave-number due to numerical damping. In this case, the numerical damping is sufficient to suppress growth of the differential model, a result which is in agreement with a previous investigation by Stewart [20].

It was shown in Section 2.3 that for finite values of interphase drag, the CATHARE differential model is also not stable within the range of wave-number investigated. However, as shown in Fig. 7, the CATHARE model when combined with the semi-implicit numerical scheme is unstable for a small range at low wave-numbers. The plot shown in Fig. 7 is for drag coefficient of 0.01 which would correspond to a flat interface. For the same conditions, the RELAP5 numerical model has similar stability behavior. One interesting difference is that the RELAP5 model predicts a growth rate which is initially greater than the basic

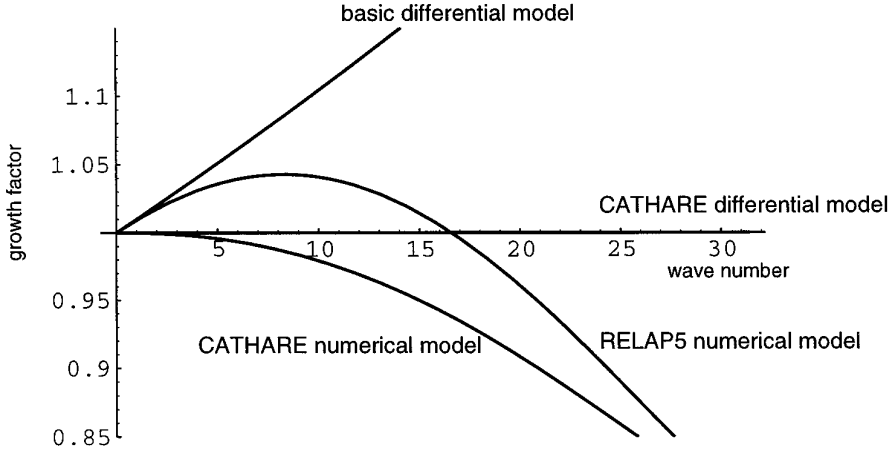

FIG. 6. Comparison between the growth factor for RELAP5 numerical model, CATHARE numerical model and the respective differential models all at zero drag.

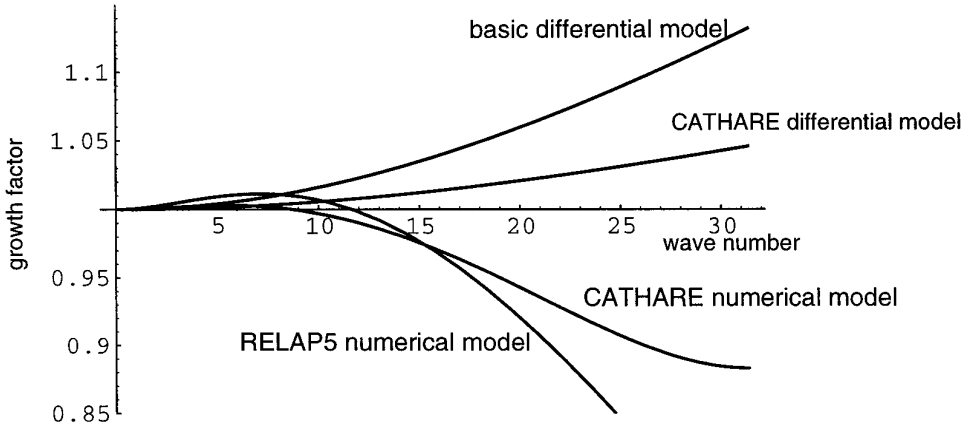

FIG. 7. Comparison between the growth rates for RELAP5 numerical model, CATHARE numerical model and the respective differential models, all at $C_d = 0.01$.

differential model, but then crosses over to become stable at higher wave-numbers. This phenomena of numerical growth factor being greater than the differential system growth factor can occur for an elliptic system of equations [21].

It is well known that a flat interface is susceptible to large wavelength instability and growth factors greater than unity for small wave-number is in agreement with this fact. However, no quantitative conclusions can be drawn about the wave-number at which the crossover from unstable to stable behavior occurs as this is the result of the complex interplay between physical and numerical modeling. Neither can this result be used directly to imply stability characteristics of the RELAP5 or CATHARE codes since special models that are not included in this analysis are used for some flow regimes.

If the drag force is increased to values which correspond to a bubbly flow, $C_d = 0.2$, then both the CATHARE and RELAP5 numerical models predict growth factors less than unity for all wavelengths. This result is shown in Fig. 8. Here again these stability results cannot be applied directly to the RELAP5 and CATHARE codes since they both use additional models such as for virtual mass force, which contribute added stability.

Physically speaking the Kelvin–Helmholtz instability can be present even for the bubbly flows at small lengthscale. In fact this instability is one of the causes of bubble disintegration. However, the wave-numbers corre-

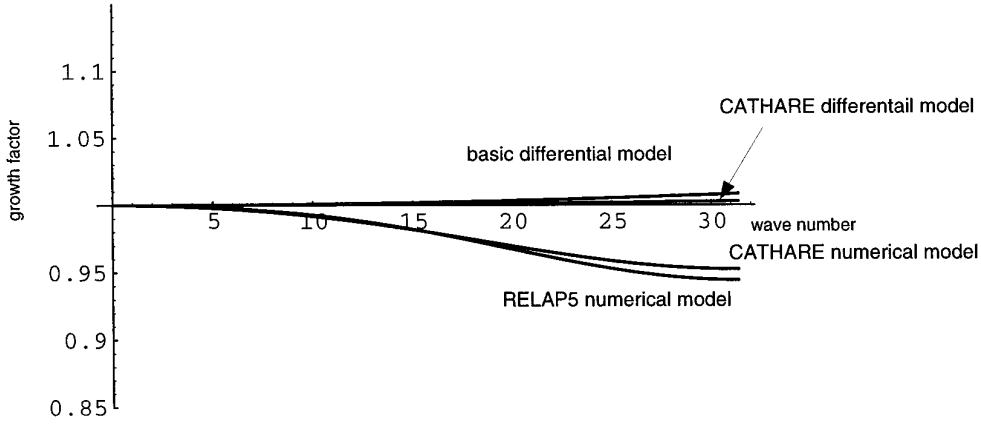

FIG. 8. Comparison between the growth factor for RELAP5 numerical model, CATHARE numerical model and the respective differential models, all at $C_d = 0.2$.

sponding to such effects are much greater than can be resolved by the averaged two-fluid model. In both the codes, the instability mechanisms are implicitly taken into consideration through algebraic constitutive relations involving surface tension and body force effects.

Shieh *et al.* [22] have conducted a RELAP5 code interphase drag sensitivity analysis. They have observed that while simulating a boiling flow experiment from subcooled to superheated conditions, void-fraction results showed oscillations in the mist flow regime, especially with finer nodalization. This is consistent with the present investigation because in the annular-mist flow regime the drag is a few orders of magnitude smaller than for bubbly flows and as depicted by Fig. 7, some growth of long wavelength solution components can occur.

4. CONCLUSIONS

Differential regularization is not retained in the basic two-fluid model for two-phase flow, due to the fact that the physical regularizing effects, i.e., surface tension and viscosity, cannot be accurately modeled. The reason for this is that the averaging process eliminates the interfacial curvature and the local velocity gradient details. These effects are included by using algebraic models which cannot represent short wavelength behavior. Thus, artificial regularization of the averaged two-fluid model is necessary. If differential regularization is not achieved in the wavenumber range of the numerical representation then regularization must be achieved as a direct result of the numerical solution process.

In this research we have shown that for two widely used two-phase flow models the predominant regularization process is numerical regardless of the mathematical character of the differential models. In the case of the CATHARE model, in which a differential term is added for the explicit purpose of regularization, i.e., making the differential system hyperbolic or parabolic, regularization still occurs as a result of the numerical process. Furthermore, the added term introduces nonphysical behavior in which the classical Kelvin–Helmholtz long wavelength instability for free slip between the phases is eliminated. Additional nonphysical effects on the velocities have been shown by other investigators [16].

In general, regularization of the averaged two-fluid model for two-phase flow must be artificially achieved. The short wavelength phenomena responsible for physical regularization cannot be accurately represented, if represented at all, for practical nodalization density. Thus, to require that the two-fluid differential model be well-posed in the mathematical sense may not be reasonable. Regularization for the cases investigated was found to be predominantly a result of the numerical process. The acceptability of this process can only be judged by assessment using experimental data.

APPENDIX

The matrices **A** and **B** are defined as

$$\mathbf{A} = \begin{bmatrix} A_{11} & A_{12} & A_{13} & A_{14} \\ A_{21} & A_{22} & A_{23} & A_{24} \\ A_{31} & A_{32} & A_{33} & A_{34} \\ A_{41} & A_{42} & A_{43} & A_{44} \end{bmatrix} \tag{A1}$$

$$\mathbf{B} = \begin{bmatrix} B_{11} & B_{12} & B_{13} & B_{14} \\ B_{21} & B_{22} & B_{23} & B_{24} \\ B_{31} & B_{32} & B_{33} & B_{34} \\ B_{41} & B_{42} & B_{43} & B_{44} \end{bmatrix} \tag{A2}$$

and the elements of these matrices are

$$A_{11} = \rho_g - \rho_f \tag{A3}$$

$$A_{12} = \frac{\alpha_g}{c_g^2} + \frac{\alpha_f}{c_f^2} \tag{A4}$$

$$A_{13} = \alpha_g \rho_g \frac{\Delta t}{\Delta x} 2i \sin\left(\frac{k\Delta x}{2}\right) \tag{A5}$$

$$A_{14} = \alpha_f \rho_f \frac{\Delta t}{\Delta x} 2i \sin\left(\frac{k\Delta x}{2}\right) \tag{A6}$$

$$A_{21} = \rho_g + \rho_f \tag{A7}$$

$$A_{22} = \frac{\alpha_g}{c_g^2} - \frac{\alpha_f}{c_f^2} \tag{A8}$$

$$A_{23} = \alpha_g \rho_g \frac{\Delta t}{\Delta x} 2i \sin\left(\frac{k\Delta x}{2}\right) \tag{A9}$$

$$A_{24} = -\alpha_f \rho_f \frac{\Delta t}{\Delta x} 2i \sin\left(\frac{k\Delta x}{2}\right) \tag{A10}$$

$$A_{31} = 0 \tag{A11}$$

$$A_{32} = \frac{\Delta t}{\Delta x} 2i \sin\left[k \frac{\Delta x}{2}\right] \tag{A12}$$

$$A_{33} = \alpha_g \rho_g (1 + \mathrm{FWG}\, \Delta t) \tag{A13}$$

$$A_{34} = \alpha_f \rho_f (1 + \mathrm{FWF}\, \Delta t) \tag{A14}$$

$$A_{41} = 0 \tag{A15}$$

$$A_{42} = -2i \sin\left[\frac{k\Delta x}{2}\right] \cdot \left(\frac{\rho_f - \rho_g}{\rho_g \rho_f}\right) \cdot \frac{\Delta t}{\Delta x} \tag{A16}$$

$$A_{43} = 1 + \mathrm{FWG}\Delta t - \rho\, \mathrm{FI}\, \Delta t \tag{A17}$$

$$A_{44} = -1 - \mathrm{FWF}\Delta t + \rho\, \mathrm{FI}\, \Delta t \tag{A18}$$

and

$$B_{11} = \rho_g - \rho_f - \rho_g v_g (1 - e^{-ik\Delta x}) \frac{\Delta t}{\Delta x} + \rho_f v_f (1 - e^{-ik\Delta x}) \frac{\Delta t}{\Delta x} \quad \text{(A19)}$$

$$B_{12} = \frac{\alpha_g}{c_g^2} + \frac{\alpha_f}{c_f^2} - \frac{\alpha_g v_g}{c_g^2} (1 - e^{-ik\Delta x}) \frac{\Delta t}{\Delta x} - \frac{\alpha_f v_f}{c_f^2} (1 - e^{-ik\Delta x}) \frac{\Delta t}{\Delta x} \quad \text{(A20)}$$

$$B_{13} = B_{14} = 0 \quad \text{(A21)}$$

$$B_{21} = \rho_g + \rho_f - \rho_g v_g (1 - e^{-ik\Delta x}) \frac{\Delta t}{\Delta x} - \rho_f v_f (1 - e^{-ik\Delta x}) \frac{\Delta t}{\Delta x} \quad \text{(A22)}$$

$$B_{22} = \frac{\alpha_g}{c_g^2} - \frac{\alpha_f}{c_f^2} - \frac{\alpha_g v_g}{c_g^2} (1 - e^{-ik\Delta x}) \frac{\Delta t}{\Delta x} + \frac{\alpha_f v_f}{c_f^2} (1 - e^{-ik\Delta x}) \frac{\Delta t}{\Delta x} \quad \text{(A23)}$$

$$B_{23} = B_{24} = 0 \quad \text{(A24)}$$

$$B_{31} = B_{32} = 0 \quad \text{(A25)}$$

$$B_{33} = \alpha_g \rho_g \left[1 - v_g (1 - e^{-ik\Delta x}) \frac{\Delta t}{\Delta x} \right] \quad \text{(A26)}$$

$$B_{34} = \alpha_f \rho_f \left[1 - v_f (1 - e^{-ik\Delta x}) \frac{\Delta t}{\Delta x} \right] \quad \text{(A27)}$$

$$B_{41} = B_{42} = 0 \quad \text{(A28)}$$

$$B_{43} = 1 - v_g (1 - e^{-ik\Delta x}) \frac{\Delta t}{\Delta x} \quad \text{(A29)}$$

$$B_{44} = -1 + v_f (1 - e^{-ik\Delta x}) \frac{\Delta t}{\Delta x} . \quad \text{(A30)}$$

REFERENCES

1. H. B. Stewart and B. Wendroff, Two-phase flows: Models and methods, *J. Comput. Phys.* **56,** 363 (1984).
2. M. Ishii, *Thermo-Fluid Dynamic Theory of Two-Phase Flow* (Eyrolles, Paris, 1975).
3. R. T. Lahey Jr. and D. A. Drew, The three dimensional time and volume averaged conservation equations of two-phase flows, *Adv. Nucl. Sci. Technol.* **20,** 1 (1988).
4. H. Tennekes and J. L. Lumeley, *A First Course in Turbulence* (MIT Press, Cambridge, MA, 1972).
5. W. Rodi, *Turbulence Models and Their Application in Hydraulics—A State of the Art Review* (Balkema, Rotterdam/Brookfield, 1993).
6. R. Krishnamurthy and V. H. Ransom, A non-linear stability study of the RELAP5/MOD3 two phase model, presented at *Japan–US Seminar on Two-Phase Flow Dynamics, Berkeley, California, 1992).*
7. M. Arai, Characteristic and stability analyses for two-phase flow equation system with viscous terms, *Nucl. Sci. Eng.* **74,** 77 (1980).
8. J. M. Delhaye, Basic equations for two-phase flow modeling, in *Two-Phase Flow and Heat Transfer in the Power and Process Industry,* edited by A. E. Bergles *et al.* (Hemisphere, Washington, 1981).
9. V. H. Ransom and D. L. Hicks, Hyperbolic two-pressure models for two-phase flows, *J. Comput. Phys.* **53,** 124 (1984).
10. V. H. Ransom *et al., RELAP5/MOD2 Code Manual, Vol. 1: Code Structure, System Models, and Solution Methods,* NUREG/CR 4312, 1985.
11. A. Prosperetti and J. V. Satrape, Stability of two-phase flow models, in *Two-Phase Flows and Waves,* edited by D. D. Joseph and D. G. Schaffer (Springer-Verlag, New York/Berlin, 1990), p. 98.
12. M. Ishii and N. Zuber, Relative motion and interfacial drag coefficient in dispersed two-phase flow of bubbles, drops and particles, *AIChE J.* **25,** 843 (1979).
13. J. D. Ramshaw and J. Trapp, Characteristics, stability and short-wavelength phenomena in two-phase flow equation system, *Nucl. Sci. Eng.* **66,** 93 (1978).
14. J. C. Micaelli, *Document De Synthese CATHARE (CATHARE An Advanced Best-Estimate Code for PWR Safety Analysis*), SETh/LEML-EM/88-129, Grenoble Cedex, 1988.
15. D. Bestion, The physical closure laws in CATHARE code, *Nucl. Eng. Design* **124,** 229 (1990).
16. I. Toumi, An upwind numerical method for a six equation two-phase flow model, *Nucl. Sci. Eng.* **123,** 147 (1996).
17. J. H. Stuhmiller, The influence of interfacial pressure forces on the character of two-phase flow model equations, *Int. J. Multiphase Flows* **3,** 551 (1977).
18. H. Lamb, *Hydrodynamics* (Dover, New York, 1945).
19. F. de Crecy, *Etude des Ecoulements Stratifies dans une Conduite,* CAE Internal Report TT, No. 169, 1981.
20. H. B. Stewart, Stability of two-phase flow calculations using two-fluid model, *J. Comput. Phys.* **3,** 259 (1979).
21. V. H. Ransom and J. Trapp, Applied mathematica models in nuclear thermal hydraulics, in *ANS/AIChE/ASME Proceedings, Nuclear Thermal Hydraulics, Feb. 1983,* Vol. 1.
22. S. Shieh, R. Krishnamurthy, and V. H. Ransom, Stability, accuracy and convergence of the numerical method in RELAP5/MOD3, *Nucl. Sci. Eng.* **116,** 227 (1994).